Phys. Status Solidi B **247**, No. 10, 2537–2549 (2010) / **DOI** 10.1002/pssb.201046181

physica status solidi b
www.pss-b.com
basic solid state physics

Feature Article

Electronic structure and magnetism of monatomic one-dimensional metal nanostructures on metal surfaces

P. A. Ignatiev[1], N. N. Negulyaev[2], L. Niebergall[1], H. Hashemi[2], W. Hergert[2], and V. S. Stepanyuk[*,1]

[1] Max-Planck-Institut für Mikrostrukturphysik, Weinberg 2, 06120 Halle, Germany
[2] Fachbereich Physik, Martin-Luther-Universität, Halle-Wittenberg, Friedemann-Bach-Platz 6, 06099 Halle, Germany

Received 15 April 2010, revised 9 June 2010, accepted 6 June 2010
Published online 9 August 2010

Keywords density functional theory, magnetic interactions, Monte Carlo simulations, nanostructures, self-assembly, surface states

[*] Corresponding author: e-mail stepanyu@mpi-halle.mpg.de, Phone: +49 345 5582645, Fax: +49 345 5511223

We report on theoretical studies of one-dimensional (1D) monatomic metal nanostructures coupled to metal substrates, which support surface states. The aim of the work is to demonstrate general features of electronic structure, magnetic properties, and interactions in such systems. We start from simple finite monatomic chains. It is shown that electronic confinement in 1D metallic chains can be observed at energies of projected band gaps of a metallic substrate. At other energies the confinement is significantly suppressed by scattering of chain states into the metallic substrate. Although this scattering decreases the exchange interaction between magnetic atoms incorporated into the chain, we show that it is still possible to get a significant enhancement of the exchange interaction in short chains. The next problem addressed in the paper is related to the interaction of the surface state with ad-chains and 1D resonators. Special attention is paid to a possible impact of confinement in 1D resonators on atomic diffusion and self-organization inside them. Finally, we illustrate the theoretical approach for the treatment of magnetization dynamics in 1D nanostructures.

1 Introduction The focus of the surface science drifts nowadays towards atomic-scale systems, e.g., wires [1–11], stripes [2, 12–18], clusters [1, 19–25], and nanodots [26–32]. Such downscaling requires realistic and efficient ways of description of systems, whose properties are determined by quantum effects and, therefore, are strongly dependent on the environment, dimension, structure, and atomic species involved [33]. Every particular class of systems should be carefully studied experimentally and theoretically in order to reveal some general phenomena. This paper is devoted to one-dimensional (1D) monatomic metal nanostructures on metal substrates. Despite the seeming simplicity of such structures, they are a perfect illustration of fundamental properties of low-dimensional quantum systems. In this paper we deal with various close-packed and sparse 1D atomic structures, which could be located on flat or stepped surfaces. Generally speaking, in all cases we are interested in electronic properties and magnetic phenomena. The next interesting aspect of our study is related to creation of low-dimensional nanostructures on surfaces [33]. They could be self-assembled in a "bottom-up" manner [1–30, 33–40], or built in a "top-down" approach by means of the scanning tunneling microscopy (STM) [41–49]. The latter technique allows to map surface topography at the atomic scale [50–53] or even with a true atomic resolution [54] and to record simultaneously spectral characteristics of the sample studied [55–57]. Scanning tunneling spectroscopy (STS) measurements can be easily compared to appropriate theoretical *ab initio* descriptions [55, 58, 59].

The paper is organized as follows. Our studies are based on the density functional theory (DFT), therefore, Section 2 describes the *ab initio* method involved. Section 3 is devoted to electronic and magnetic properties of monatomic chains on metal surfaces. In Section 4 we introduce quantum resonators and describe how 1D electronic confinement in resonators governs the atomic diffusion. In Section 5 we concentrate on the magnetization dynamics of 1D nanostructures. We present a model based on the Heisenberg Hamiltonian and then apply it to investigate ferromagnetism of close-packed and sparse 1D atomic structures.

2 KKR Green's function method Electronic properties of systems presented in this paper were calculated by means of the Korringa–Kohn–Rostoker (KKR) Green's function method, so it is worthwhile to introduce it. The KKR is an ideal tool for *ab initio* description of impurities embedded into a crystal or placed on a surface. The KKR Green's function method is the implementation of the DFT. It exploits the multiple scattering formalism to solve Kohn–Sham equations formulated in the DFT framework. Mathematically, the KKR method rests on two facts [60]: (i) the local density of states (LDOS) $\rho(\mathbf{r},\varepsilon)$ is connected to the Green's function $G(\mathbf{r},\mathbf{r}',\varepsilon)$ of a system as:

$$\rho(\mathbf{r},\varepsilon) = -\frac{1}{\pi}\,\mathrm{Im}\,G(\mathbf{r},\mathbf{r},\varepsilon), \tag{1}$$

and (ii) the Green's function $G(\varepsilon)$ of a perturbed system can be expressed from the Green's function $\overset{\circ}{G}(\varepsilon)$ of the reference system by means of the Dyson equation:

$$G(\varepsilon) = \overset{\circ}{G}(\varepsilon) + \overset{\circ}{G}(\varepsilon)T(\varepsilon)\,\overset{\circ}{G}(\varepsilon), \tag{2}$$

where $T(\varepsilon)$ is the so-called transition matrix (or T-matrix) relating the states $|\Psi\rangle$ of a perturbed system to the states $|\Psi_0\rangle$ of the unperturbed one. The T-matrix is defined as $V|\Psi\rangle = T(\varepsilon)|\Psi_0\rangle$, where V is a perturbing potential. Such a construction makes it possible to express any perturbed system in terms of the reference one [61, 62]. More precisely, a bulk crystal is treated as a periodical three-dimensional (3D) perturbation of the free space. The Dyson equation in this case is formulated in the reciprocal space. A surface, accordingly, can be considered either as a 2D perturbation of an infinite bulk crystal, or as a 2D slab, which perturbs the free space. Finally, a finite cluster is a real space perturbation of an infinite surface and, therefore, can also be studied by means of the KKR. The shape and the size of a region perturbed by the cluster at the surface are not restricted to some method-related parameters, like supercell size in plane-wave codes, hence systems spread over several nanometers can be studied by the KKR [63–65]. Finally, the KKR method, as we show below, allows straightforward calculations of the magnitude of interactions mediated by conduction electrons.

It is worth to notice, that atomic chains on surfaces have also been studied by theoretical methods other than KKR, like, self-consistent tight-binding method [66–68], real space linear muffin tin orbital method in atomic sphere approximation [69], plane-wave based codes [70, 71], and wave-packet propagation method [72, 73].

3 Monatomic chains on metal surfaces Monatomic chains are the simplest 1D metal nanostructures on a metal substrate. They can be created by means of STM manipulations [44, 45, 47–49]. The undoubted merit of this technology is the ability to create chains from several species in an atom-by-atom fashion thus controlling both their layout and composition [44, 45, 47–49]. In this section we review the most important experimental and theoretical results on monatomic metal chains on metal surfaces. We focus our attention on the electronic structure of chains and consider magnetic interactions inside and between them.

3.1 Confinement in chains An isolated metallic chain can be described at the first approximation by the particle-in-a-box model. The electronic spectrum of such a *confined* system is characterized by a set of *discrete* energy levels, whose energies ε_n depend on the length L of the chain as $\varepsilon_n = \hbar^2/2m(\pi n/L)^2$, where m is the electron mass. The corresponding electronic density of state n is characterized by:

$$\rho_n(x) = \frac{2}{L}\sin^2\left(\frac{n\pi x}{L}\right), \tag{3}$$

and exhibits n peaks. Electronic states in gaps between these levels are not allowed. If a metal chain is placed on a metal surface, then the interaction of chain states with substrate conduction electrons has to be taken into account. At a first glance, such an interaction could result in vanishing gaps in the chain's electronic structure and in the loss of the confinement as states prohibited in chain gaps could be allowed in the substrate. This statement does not imply that the confinement in metal chains on metal surfaces is fundamentally impossible. It only suggests, that in order to retain the chain-confined states, it is necessary to significantly limit their interaction with substrate electrons. Such "decoupling" of chain and substrate states can occur, for example, if the chain-confined states fall into the projected gap of the substrate electronic structure. This point has recently been demonstrated by means of the STM/STS studies.

First STM/STS experiments on confined states of artificial monatomic chains were performed by Fölsch et al. [47]. Close-packed Cu chains were assembled on Cu(111) by means of atomic manipulations. Investigations of chains electronic structure by means of STS revealed series of unoccupied states manifesting themselves as peaks in scanning tunneling spectra [47]. Number of peaks, their energies and spatial localization were found to depend on the chain length [47]. The state with the lowest energy is localized spatially in a single node at the center of a chain. Then eigenstates with two distinct nodes were observed at a higher energy; then – with three nodes, etc. Such a development of the electronic structure is typical for the particle-in-a-box model (3) [47].

3.2 Bound states Electronic confinement in metal ad-chains manifests itself at energies of the projected bulk band gap of the substrate where the coupling between the chain-confined and substrate states is small. Now we are going to address the so-called bound states, which appear due to perturbation of the substrate electronic structure by an ad-chain. To treat this problem correctly, we should introduce the so-called surface state of Cu(111).

Electrons inside a crystal obey the Bloch theorem and can occupy only the allowed set of energies separated with

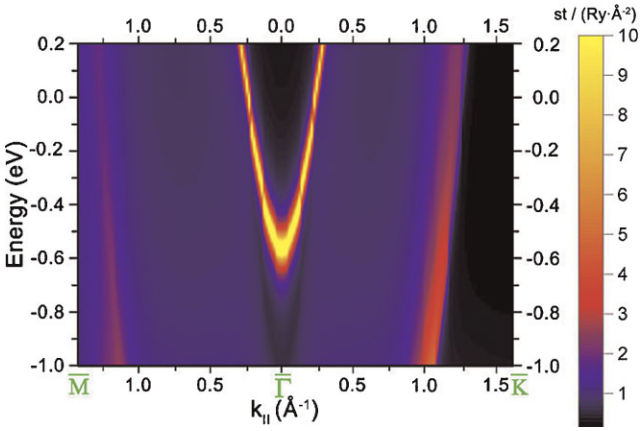

Figure 1 (online color at: www.pss-b.com) The energy resolved spectral density map calculated at the interface layer of the Cu(111) surface along $\overline{\mathrm{M}} - \overline{\Gamma} - \overline{\mathrm{K}}$ direction of the 2D Brillouin zone. Blue and violet areas correspond to the projected bulk bands. Black regions are gaps of the projected band structure. The surface state band is presented as a bright parabola with a band bottom at −0.536 eV.

band gaps. Break of the crystal symmetry at a surface changes the spectrum and causes additional bands to appear in the gaps of the bulk band structure. States described by such bands are confined at the surface in between the vacuum potential barrier on the one, and the crystal band gap on the other side [74, 75]. The dispersion law of such surface states depends on the type and the position of the gap. The surface state arising in the inverted $\overline{L}$-gap of the bulk Cu is 2D-free-electron-like and is described by a parabolic dispersion relation [76]: $E(\boldsymbol{k}_{\parallel}) = E_0 + \hbar^2/2m \cdot \boldsymbol{k}_{\parallel}^2$, where $\boldsymbol{k}_{\parallel}$ is the in-plane wave vector and E_0 is the surface state band bottom. Figure 1 demonstrates the spectral density map of electronic states of the interface layer of the Cu(111) surface calculated along $\overline{\mathrm{M}} - \overline{\Gamma} - \overline{\mathrm{K}}$ direction of the Cu(111) 2D Brillouin zone by means of the KKR method. Black areas of the spectral density map correspond to the projected bulk band gaps. One gap is situated at the $\overline{\Gamma}$-point, another is visible at the $\overline{\mathrm{K}}$-point. Blue and violet areas are projected bulk states of bulk Cu. Bright parabolic band at $\overline{\Gamma}$ with the bottom at the energy of approximately −0.536 eV is the Cu(111) surface state. The Fermi wavelength of the surface state $\lambda_{\mathrm{F}}^{\mathrm{ss}} = 26.6$ Å ($\boldsymbol{k}_{\mathrm{F}} = 0.235$ Å^{-1}) is much larger than that of bulk states ($\lambda_{\mathrm{F}}^{\mathrm{b}} = 4.62$ Å). Note, that the broadening technique applied to facilitate the convergence results in blurring of gap edges and in the broadening of the surface state band in Fig. 1.

It is clear that the interaction of a 2D surface state with ad-structures could be very much different from the case of 3D Cu bulk states. This difference can be derived using the extended Newns–Anderson model describing an adsorbate interacting with bulk Bloch states and with the surface state [77, 78]. It can be demonstrated, that any feature in the density of substrate states induces a state localized at the adatom. Bulk states are featureless; the density of the surface state has an onset at the energy of the surface state band bottom. The interaction of the surface state with an adsorbate produces a bound state resonance below the surface state band bottom [78]. The bound state resonance obtained by means of the KKR method for a Cu adatom on the Cu(111) surface [79] is demonstrated in Fig. 2a. It is most pronounced above the adatom, then, moving away from the atom, its density rapidly decreases, and at 10.2 Å from the adatom the LDOS turns into the LDOS of clean Cu(111). Several experimental studies have revealed such kind of bound states above adatoms on Cu(111) and Ag(111) [78, 80]. We refer the reader to these works for details.

Ad-chains also produce bound states. A chains, as opposed to an adatom, cannot be considered to be a point perturbation coupled to the Cu(111) surface state. Elongated shape of chains and the mutual coupling of their atoms results in the formation of rather complex bound states resembling standing waves arising in confined geometries. Figure 2b presents LDOS calculated above various parts of the Cu chain consisting of seven atoms aligned along $\langle 10\overline{1} \rangle$ direction on the Cu(111) surface [79]. Although a broad bound state resonance is clearly visible in all three cases, its energy significantly depends on the position along the chain. Bound states localized at chain edges (Fig. 2b, position 1) resemble adatom bound states shown in Fig. 2a. But as one

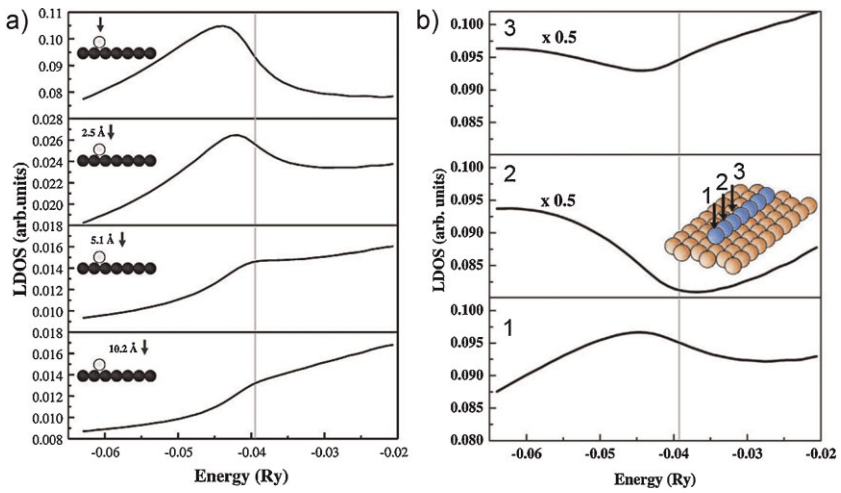

Figure 2 (online color at: www.pss-b.com) (a) The LDOS over the Cu adatom on Cu(111) at different lateral distances. Gray line corresponds to the energy of the surface state band bottom. Bound state appears below this energy. Bound state is most pronounced above the adatom and decays with distance. (b) The change in the LDOS along the Cu chain. Bound state in the central part of the chain is localized at lower energies than that at the chain edges [79].

moves towards the chain center (Fig. 2b positions 2, 3), bound state resonances abruptly move to lower energies. Edge atoms are coupled to a single neighbor, while atoms inside the chain are coupled to a pair of neighbors. Different coupling strengths could explain variations in energy of bound states at edges and in the center.

3.3 Magnetic interactions All the systems we have considered so far have been nonmagnetic. Now we are going to extend our reasoning to chains with incorporated magnetic atoms. Such structures can be fabricated by means of either the self-assembly [39, 40], or atomic manipulations [49]. In the first, "bottom-up" approach, the Pt(997) vicinal surface has been used as a template for the growth of mixed 1D chains [39, 40]. In the second case, magnetic Co atoms were evaporated on the Cu(111) surface, and then, by means of STM manipulation, mixed chains were assembled from Co and Cu atoms. The latter were produced by tip indentation [49]. Fabricated chains were then studied by means of the STS. It was demonstrated that it is possible to resolve the position of Co atoms in the chain. It was revealed that Co doping allows to tune unoccupied confined states of the chain. Here, we are going to discuss the exchange interaction between magnetic atoms incorporated into the chain and the exchange interaction between magnetic chains.

The exchange interaction between magnetic atoms coupled to a metal substrate is mediated by substrate conduction electrons. Let us suppose that we have a pair of magnetic impurities. Electrons scattered off both magnetic impurities interfere with each other. Since scattering at magnetic impurities is spin-dependent, the interference patterns for parallel (P) and antiparallel (AP) alignment of magnetic moments of impurities are also different. The resulting total energies of P and AP systems are not degenerate and one of these configurations is energetically more favorable by the energy $\Delta E = E_{\mathrm{P}} - E_{\mathrm{AP}}$:

$$\Delta E = \int_{-\infty}^{E_{\mathrm{F}}} \mathrm{d}\varepsilon(\varepsilon - E_{\mathrm{F}})\,\Delta\rho(\varepsilon), \tag{4}$$

where E_{F} is the Fermi energy and $\Delta\rho(\varepsilon) = \Delta\rho^{\mathrm{P}}(\varepsilon) - \Delta\rho^{\mathrm{AP}}(\varepsilon)$ is the total interference-related DOS difference between P and AP configurations. The total change of the DOS $\Delta\rho(\varepsilon)$ can be expressed using explicit terms $\Delta\rho_{\sigma_1,\sigma_2}$ for density of conduction electrons of particular spin characters ($\sigma_i = \{\uparrow,\downarrow\}$) scattered at impurities 1 and 2. In P configuration the change of DOS reads $\Delta\rho(\varepsilon)^{\mathrm{P}} = \Delta\rho(\varepsilon)_{\uparrow\uparrow} + \Delta\rho(\varepsilon)_{\downarrow\downarrow}$, where the first and the second terms describe the scattering of majority and minority electrons, respectively. In AP configuration the majority and minority scattering properties of the second impurity are swapped and $\Delta\rho(\varepsilon)^{\mathrm{AP}} = \Delta\rho(\varepsilon)_{\uparrow\downarrow} + \Delta\rho(\varepsilon)_{\downarrow\uparrow}$. The total change of DOS can be expressed as:

$$\Delta\rho(\varepsilon) = \Delta\rho_{\uparrow\uparrow} + \Delta\rho_{\downarrow\downarrow} - \Delta\rho_{\uparrow\downarrow} - \Delta\rho_{\downarrow\uparrow}. \tag{5}$$

Each term of this sum can be formulated in terms of scattering matrices $T_{\sigma_1\sigma_2}$:

$$\Delta\rho_{\sigma_1\sigma_2} = -\frac{1}{\pi}\,\mathrm{Im}\,\mathrm{Tr}\ln[T_{\sigma_1\sigma_2}(E_{\mathrm{F}})]. \tag{6}$$

This equation, also known as Lloyd's formula [60], is in the spirit of the KKR Green's function method (see Eq. (2)) and can be directly implemented in it. The sign of the exchange energy ΔE depends on scattering properties of magnetic impurities incorporated in $T_{\sigma_1\sigma_2}$. The Fermi wavelength of conduction electrons, their density and dimensionality are of great importance. Indeed, the interaction between two single bulk impurities mediated by bulk Bloch states decays as $\propto 1/r^5$ [81], while the surface state mediated interactions obey the inverse quadratic law $\propto 1/r^2$ [82]. Below we demonstrate how atomic chains can be used to tailor the exchange interaction.

3.3.1 Mixed chains At first we present the exchange interaction (see Eq. (4)) between a pair of Cr atoms on the clean Cu(111) surface. It is plotted in Fig. 3a with a dashed blue line [83]. The nearest neighbor Cr dimer exhibits strong antiferromagnetic coupling promoted by a direct overlap Cr d-shells filled with four electrons. At larger separation of 5.1 Å the direct overlap is much smaller and the interaction is mediated by substrate electrons. As a result, the magnitude of the exchange interaction is strongly reduced and its sign is changed. At further separations the exchange interaction, oscillating, decays to 0. The decay rate of the oscillations envelope $\propto r^{-2}$ at large separations is determined by the surface state.

Let us trace now the effect of a Cu chain linking Cr atoms. The exchange interaction of a pair of Cr adatoms at a separation of 5.1 Å with a single Cu adatom inserted as a link between them is slightly reduced in comparison to the reference case of single unlinked Cr adatoms. But already two Cu atoms linking a Cr pair reverse the sign of the

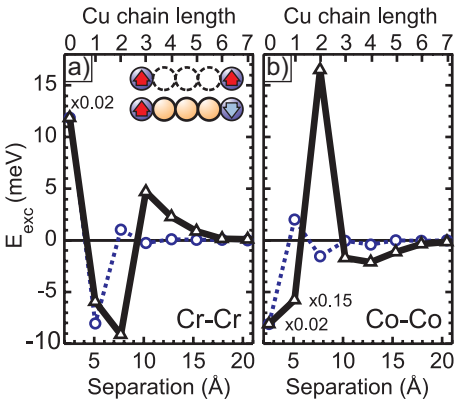

Figure 3 (online color at: www.pss-b.com) (a) The exchange interaction between two single Cr atoms on the Cu(111) surface (dotted blue line, open circles) and the exchange interaction between those atoms linked with a nonmagnetic Cu chain (solid black line, open triangles). (b) The same dependencies for a Co pair [83].

exchange interaction and strongly enhance its magnitude. The system with three Cu atoms in the chain has the antiferromagnetic exchange interaction equal to 5 meV, which is about ten times larger than the corresponding magnitude of the ferromagnetic exchange interaction in the reference system. Further elongation of the chain length results in a rapid decay of the exchange interaction, which becomes smaller than the exchange interaction between single adatoms on the clean surface.

As the second example we present in Fig. 3b a comparison of the exchange interactions of two separated and two linked Co adatoms. Exact values differ from the case of the Cr pair but the general trend is the same. Enhancement of the exchange interaction in short chains and its rapid decay in long ones are general effects for various magnetic impurities. Rapid decay can be explained by the scattering of conduction electrons from the chain into the bulk. Such a scattering effectively decreases the density of interference patterns between two impurities and they get decoupled. At the same time, the density of conduction electrons at Cu atoms is much higher than that of the surface state, so interference effects are expected to be more pronounced and therefore exchange energies can reasonably be higher at separations, where the fraction of the electrons being scattered into the bulk is small [83].

Despite the small values of the reported exchange interactions, they can be probed experimentally by means of the STS. The first available method is based on the analysis of the Fano resonance, originating from the Kondo screening of magnetic impurities by conduction electrons and the formation of a singlet correlated state. This idea was initially tested on Co dimers on Au(111) [84] and then extended and improved by Wahl et al. [85] for Co atoms on Cu(001). In the second method suggested by Meier et al. [59] the exchange coupling is extracted from the magnetization curves acquired at single adatoms by means of the spin-polarized STS.

3.3.2 Interaction between chains A similar reasoning is valid for the interaction of two purely magnetic chains of length N coupled to the Cu(111) substrate (see Fig. 4, inset). The exchange interaction per chain atom $E_{\mathrm{exc}/N}$ scales linearly with N, and for $N \gg 1$ rapidly converges to a limit demonstrated in Fig. 4 with dashed line [86]. Following the hint developed for adatoms, the exchange interaction between magnetic chains can be significantly enhanced by filling the space between magnetic adatoms by the host material. As a result, chains become embedded into the substrate. The corresponding exchange interaction is presented in Fig. 4 with black solid line. At intermediate distances of $\sim$1 nm, it is one order of magnitude stronger than in the case of ad-chains. This enhanced exchange interaction promoted by surface conduction electrons has recently been proposed [86] as the origin of the ferromagnetic ordering in assemblies of Fe magnetic nanodots observed experimentally by means of magneto optical Kerr effect [26–28].

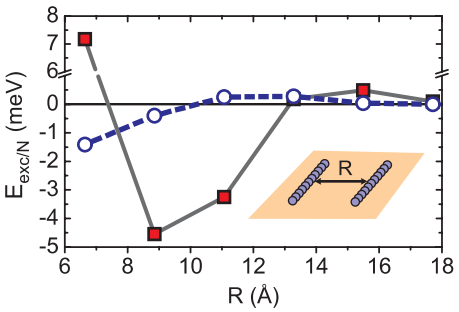

Figure 4 (online color at: www.pss-b.com) Exchange interaction $E_{\mathrm{exc}/N}$ between two parallel Fe chains divided by the total number N of atoms in a chain in the limit of long chains $N \gg 1$. Circles and dashed line demonstrate the exchange interaction between two ad-chains, squares and solid lines – between two embedded chains [86].

4 Quantum resonators One-dimensional atomic structures can be used for tailoring and controlling atomic diffusion on surfaces supporting surface-state electrons. It is well known, that scattering of such electrons off surface impurities could give rise to a valuable interaction between them. Such kind of interaction has been predicted by Lau and Kohn [81], but only recently the surface-state mediated interaction has been detected experimentally [25, 87–93]. It was revealed that surface-state mediated interactions allow one to grow ordered arrays of adatoms [35–38, 90, 91, 94–97]. In this section we focus on the effect of the 1D quantum confinement of surface states on atomic diffusion and self-organization.

4.1 Surface state-mediated interaction A substrate-mediated interaction between a pair of impurities on a surface can be formulated in the form of Eq. (4) if $\Delta\rho(\varepsilon)$ means the difference of the total DOS between a pair of coupled $(1+2)$ and decoupled (1,2) impurities:

$$\Delta\rho(\varepsilon) = \Delta\rho_{1+2} - \Delta\rho_1 - \Delta\rho_2. \tag{7}$$

At large impurity separations r ($r \gtrsim 2$ nm), the interaction is mediated by surface state electrons and for two adatoms of the same species reads exactly [82]:

$$E^{\mathrm{SS}}(r) = A_0 \left(\frac{2\sin\delta_0}{\pi}\right)^2 \frac{\sin(2\boldsymbol{k}_{\mathrm{F}}r + 2\delta_0)}{(\boldsymbol{k}_{\mathrm{F}}r)^2}, \tag{8}$$

where $\boldsymbol{k}_{\mathrm{F}}$ is the surface state Fermi wavevector, δ_0 is the phase shift, and A_0 is the scattering amplitude [42].

At intermediate separations 1 nm $\lesssim \rho \lesssim$ 2 nm, the contribution from bulk states becomes important. The interaction potential between two Fe adatoms on the Cu(111) surface calculated by means of the KKR Green's function method [98] is demonstrated in Fig. 5. It has an oscillatory behavior. The energy minimum at 2.5 Å corresponding to the close packed Fe dimer is followed by an energy barrier noted in Fig. 5 by letter A. The second interaction minimum B is situated at $\sim$12 Å and it is bounded on the right by the second repulsive barrier C. If an adatom is trapped in the minimum B,

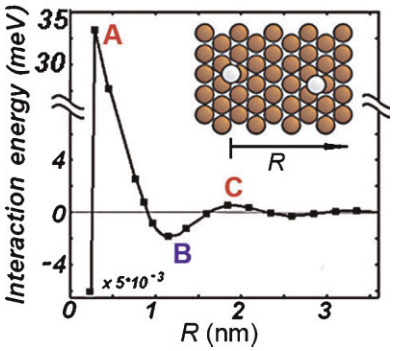

Figure 5 (online color at: www.pss-b.com) Plot of the substrate-mediated long-range interaction between two Fe adatoms on the Cu(111) substrate as a function of distance R [98].

it has to overcome either barrier A or barrier C to escape. It could be possible to stabilize the adatom at the position of minimum B by adjusting its kinetic energy, e.g., by changing the temperature. Indeed, the rate $\nu_{\alpha\to\beta}$ of an adatom-hopping between nearest hollow sites α and β of the Cu(111) surface can be written using the Arrhenius law:

$$\nu_{\alpha\to\beta} = \nu_0 \exp\left(-\frac{\Delta E_{\alpha\to\beta}}{k_B T}\right), \tag{9}$$

where T is the substrate temperature, k_B is the Boltzmann constant, and ν_0 is the hopping attempt frequency, a value of the order of 10^{12} Hz. The hopping barrier $\Delta E_{\alpha\to\beta}$ is comprised from two contributions $\Delta E_{\alpha\to\beta} = E_D + E_{SS}$. The first, E_D, is the barrier of adatom diffusion on a clean surface. The second, E_{SS}, reflects the impact of the surface state-mediated interaction on the hopping barrier and can be written as $E_{SS} = (E_\beta^{SS} - E_\alpha^{SS})/2$, where E_α^{SS} and E_β^{SS} are energies of the surface-state mediated interaction with other surface imperfections calculated for the adatom situated at hollow sites α and β, respectively. Such approximation has been verified in a number of recent studies [91, 93, 95–104]. The small variation E_{SS} of the hopping barrier E_D becomes crucial at low temperatures (1–10 K) and can effectively govern the atomic diffusion. In particular, the surface state-mediated interaction results in formation of well-ordered 2D hexagonal atomic superlattices [35–38, 97]. Below we demonstrate how the 1D quantum confinement affects the atomic diffusion.

4.2 Effect of quantum confinement on atomic diffusion Adatoms interact via surface states with all kinds of surface imperfections, like, vacancy holes, clusters, steps, and 1D chains. All such defects perturb the surface states and this perturbation affects the atomic diffusion. For example, density of surface states scattered off a long Cu atomic chain on Cu(111) represents decaying standing waves parallel to the chain. STM observations have recently revealed that a Cu adatom placed near such a chain prefers to migrate along the channel of increased density of surface states [104]. We demonstrate below that this phenomenon is related to the surface-state mediated interaction and leads to a self-organization of a novel class of 1D nanostructures stabilized by this interaction.

4.2.1 Fe nanostrings on a stepped Cu surface Interaction energies between a Fe adatom and ascending and descending Cu steps on Cu(111) are presented in Fig. 6a and b [98]. One can see that the interaction energy in both cases is oscillatory with a period of about 1.5 nm (half of the Fermi wavelength of the surface state on Cu(111)). The adatom moving towards a step is repelled by the repulsive potential. For the lower and upper terraces, the first repulsive barrier occurs at distances of about 0.4–0.5 nm from the step. The strength of this repulsive potential on the upper terrace (173 meV) is significantly larger than that for the lower terrace (26 meV). The physics underlying the difference in behavior of adatoms at the upper and the lower terraces is related to a redistribution of the electron-charge density at step edges as was suggested long ago by Smoluchowski [105].

Let us first examine the thermal diffusion of an individual Fe adatom on a terrace of a stepped Cu(111)

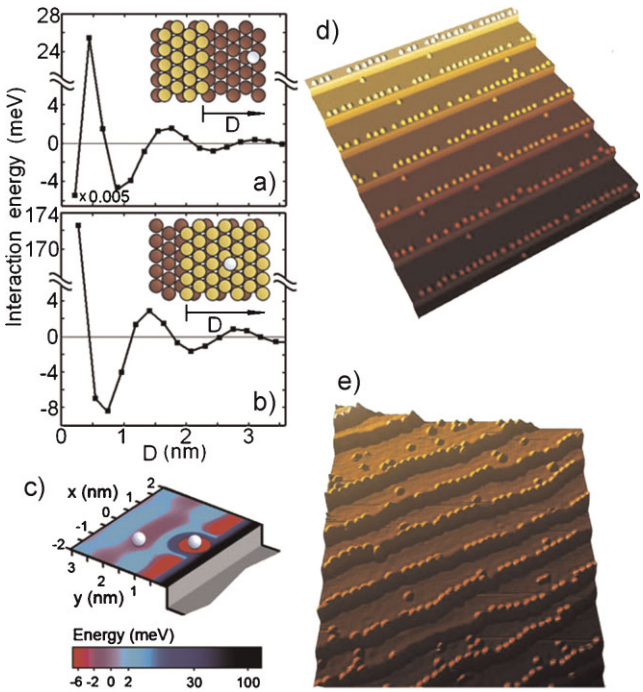

Figure 6 (online color at: www.pss-b.com) The interaction energy between a Fe adatom and Cu steps on Cu(111): (a) for the lower terrace and (b) for the upper terrace. The interaction energy at 2.2 Å in (a) is scaled by 0.005. (c) The 2D potential-energy map for the Fe adatom to approach another Fe adatom trapped in the potential well near the edge of the upper terrace. (d) The kMC simulations of the self-organization of Fe adatoms on a vicinal Cu(111) into atomic strings. Calculations are performed according to the experimental conditions. (e) The STM image of Fe atomic strings on the vicinal Cu(111) surface. The size is 40×40 nm^2, Fe coverage is 0.008 ML, the temperature of the system is 12 K. Imaging conditions: $V = -0.8$ V and $I = 1$ nA [98].

surface at a temperature of about 10 K. The first minimum of the interaction energy is found to be at ∼0.7 nm on the lower terrace and at ∼0.8 nm for the upper terrace. The depth of the first attractive minimum on the upper terrace (∼8 meV) is twice larger compared to that on the lower terrace (∼4 meV). A simple estimation by means of Eq. (9) yields, that at $T = 10$–13 K the occupation probability of surface sites in the potential well near the edge of the upper terrace is about 100 times larger than that on the lower terrace. Hence, it seems likely that the preferential adatom position at such temperatures is on the upper terrace at about 0.7 nm from the descending step edge.

Let us now assume that there are several Fe adatoms diffusing on a terrace of stepped Cu(111). Adatoms captured near the descending step edge should interact with each other. In Fig. 6c we depict the potential-energy map for the Fe adatom approaching another Fe adatom trapped in the potential well near the descending step edge [98]. The repulsive area surrounding this adatom is well seen. It is easier for the Fe adatom to approach the step edge within a distance of about 1.2 nm from the first Fe adatom. Fe adatoms interacting with the descending step edge and with each other, thus, could form a sparse atomic string with interatomic distances around 1.2 nm. This assumption was confirmed both theoretically and experimentally by means of kinetic Monte Carlo (kMC) [106] simulations and the STM. Figure 6d demonstrates the result of our kMC simulation. Fe atoms situated 0.7 nm away from the step edge with the average interatomic separation equal to 1.2 nm form quasi 1D atomic strings at step edges. An STM image of Fe adatoms evaporated on the Cu(111) stepped surface at 12 K is demonstrated in Fig. 6e [98]. Sparse 1D chains are clearly visible.

4.2.2 Self-organization in 1D confined geometries Now we turn to the atomic diffusion inside 1D quantum resonators. Such structures can be of a natural origin. For example, a resonator can be comprised from two monatomic steps [107]; resonators can be assembled in an atom by atom fashion by means of the STM [104], or they can be self-organized [10, 108, 109]. Surface state electrons get confined to resonators and form standing waves, which could be described in a crude approximation by Eq. (3). Figure 7a demonstrates a Cu resonator fabricated on the Cu(111) surface by STM manipulations [104]. The distance between the resonator chains is 55 Å. Standing LDOS waves with three maxima are clearly visible inside the resonator. To calculate the interaction energy of an adatom with resonator walls, one has to be sure that the LDOS is reproduced correctly by the theoretical method used. Figure 7b provides comparison of the LDOS obtained by means of the KKR Green's function method with the result of STS measurements [104]. The agreement between theory and experiment is very good.

Figure 7c presents the 2D potential energy map of a Cu adatom placed in different hollow sites inside the resonator [104]. The zero energy in Fig. 7c corresponds to the energy of the adatom on the clean flat Cu(111) surface, so the energy map represents the interaction potential of the adatom with the resonator walls. The interaction exhibits oscillatory behavior in the direction perpendicular to the chains. If the adatom is situated at the first nearest neighbor separation from a chain, the interaction is strongly attractive due to the direct bonding and is equal to −1.25 eV. Then, there is a repulsive barrier of 33 meV at 4–9 Å from the chain, which prevents at low temperatures the nucleation of the adatom with the chains. The area of attractive interaction of −6 meV is situated at 9–15 Å. It is separated from the next attractive area of −1 meV at the center of resonator by a small repulsive barrier of 2 meV at 16–23 Å.

In order to quantify the effect of the interaction potential shown in Fig. 7c on the atomic diffusion, the kMC study was performed [104]. In each kMC trial the Cu adatom was initially placed in the random hollow site inside the

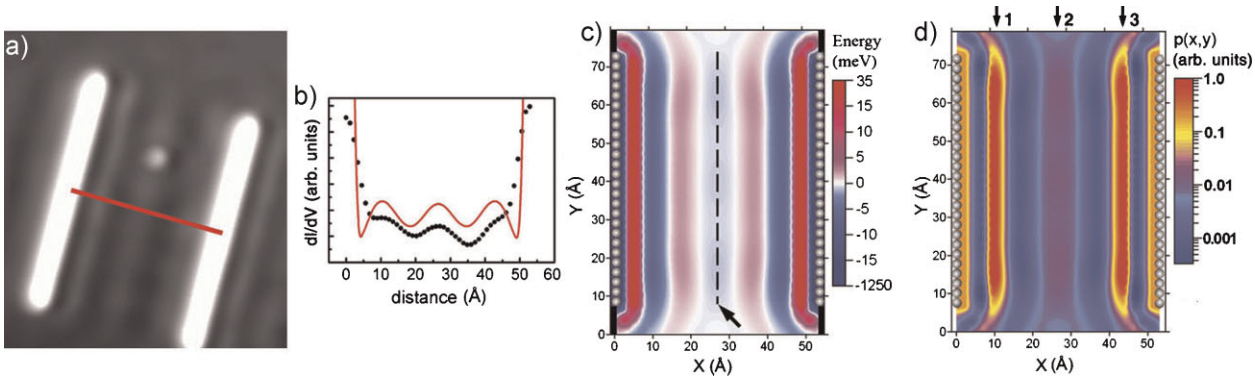

Figure 7 (online color at: www.pss-b.com) (a) A single Cu adatom inside a quantum resonator built from two parallel monatomic Cu chains on Cu(111). The distance between the chains is 55 Å. $T = 12$ K, $I = 0.07$ nA, $V = +0.1$ eV. Image size 100×100 Å^2. (b) Experimentally measured dI/dV signal at $V = +0.05$ eV (black dots) and the calculated LDOS at the Fermi level (red curve) perpendicular to the resonator walls [red line in (a)]. (c) The 2D map of the interaction potential between a Cu adatom and the quantum resonator (two parallel monatomic Cu chains with interchain separation of 55 Å). The black dashed line marks the central line of the resonator. (d) The probability density of finding the randomly walking Cu atom inside the resonator at 12 K. Three diffusion channels (the areas, where an adatom can be found with a high probability) are marked with the enumerated arrows [104].

resonator, and its movement was simulated at $T = 12$ K. Finally, the probability density of finding the adatom at hollow site (x, y) was calculated as $\rho(x, y) = t_{x,y} / \sum_{i,j} t_{i,j}$, where $t_{i,j}$ is the total time, which the adatom spends in hollow site (i,j) [106]. Both fcc and hcp sites were considered during simulations, and the summation was performed over all possible hollow sites. The calculated probability density is presented in Fig. 7d. If we exclude adatoms nucleated with chains, there are three areas with a high probability to find the adatom. These channels of adatom diffusion correspond to the areas of the negative interaction energy. If the adatom is placed into such a channel, then at $T = 12$ K it diffuses predominantly parallel to the resonator walls. If the adatom is introduced between the channels, it first diffuses towards one of the channels and then migrates inside it parallel to the resonator walls. As can be seen from Fig. 7c and d channels are closed, i.e., areas of attractive potential exist only inside the resonator and do not spread out of it. As a result, adatoms get trapped within the resonator due to the 1D confinement.

When a number of adatoms is placed simultaneously inside the resonator, one can expect that the interaction between them could result in the formation of sparse string-like structures similar to those shown in Fig. 6d and e. Such structures have been recently observed inside methionine molecular nanogratings self-assembled on the Ag(111) surface [10, 108, 109]. The methionine amino-acid deposited onto Ag(111) at ~320 K self-assembles into regular 1D nanogratings aligned along the ⟨110⟩ direction of the substrate. The interchain separation can be tuned within 20–200 Å at molecular coverages between 0.1 and 0.6 ML [109]. Each chain consists of two molecular rows dimerized by means of hydrogen bonds [109]. Each row is also stabilized by means of hydrogen bonds [109]. The amino-acid grating perturbs the Ag(111) surface state acting on it as a potential barrier. The surface state gets confined to the patches of the clean Ag(111) surface between molecular chains and each trench, thus, can be considered as a very long quantum resonator.

Figure 8a demonstrates the surface-state mediated interaction between the adatom and the walls of the resonator calculated by means of the KKR Green's function method. Scattering of surface state electrons at nanogratings was simulated by scattering at Ag chains. The average effective width of the potential well between scatterers was 50 Å. Interactions presented in Fig. 8a for Co and Fe adatoms are almost identical and both have the only attractive minimum in the center of resonator [108].

The long-range substrate-mediated interaction between a pair of adatoms within the examined resonator is plotted in Fig. 8b. It has an attractive minimum at separations of ~26 and ~23 Å for Co and Fe adatoms, respectively. Finally, Fig. 8c demonstrates the 2D energy landscape showing both adatom–resonator and adatom–adatom interactions. According to this result, it is most favorable energetically for a Co adatom to stay at the center of the resonator at a distance of ~25 Å from another adatom. Figure 8d demonstrates an

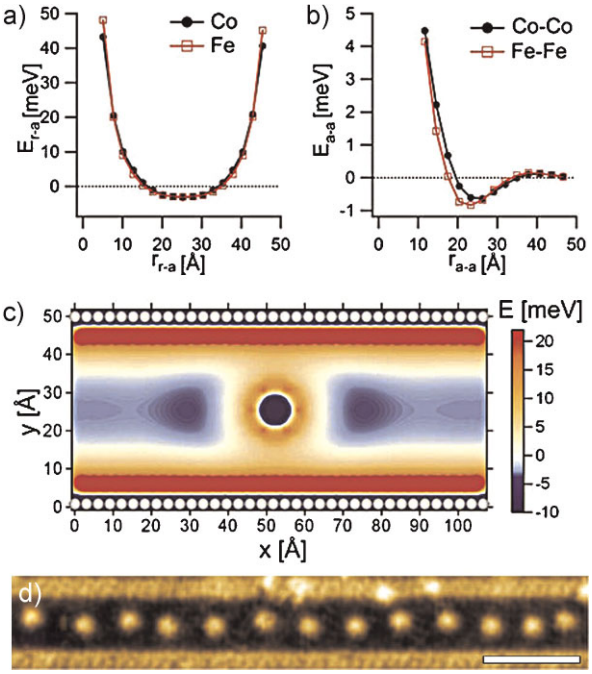

Figure 8 (online color at: www.pss-b.com) (a) KKR Green's function calculations of the interaction energy between Fe and Co adatoms and a quantum resonator built from two parallel Ag atomic chains. (b) Adatom–adatom interaction potential along the symmetry axis of the resonator revealing preferential spacings of ~26 Å for Co and ~23 Å for Fe, respectively. (c) 2D map of the interaction potential calculated for the quantum resonator and one Co adatom positioned in the middle of the resonator. (d) STM topography of Co adatoms self-organized in 1D sparse nanostructure in between biomolecular trenches. Image acquired at 12 K after annealing to 18 K ($I = 0.06$ nA, $U = -1.770$ V). Scalebar corresponds to 50 Å [108].

STM study of the atomic self-alignment of Co inside biomolecular gratings. Adatoms really form elongated sparse assemblies. Statistical study of the movement of Co adatoms at 18 K confirmed their nonrandom positioning inside the trench. The probability density of finding an adatom is maximal in the center of the trench at ~25 Å from its neighbors [108]. These values are in remarkable agreement with the theory.

5 Magnetic properties of 1D chains In Section 3.3 we presented our results on the exchange interaction between a pair of magnetic impurities. Looking at Fig. 3 one can conclude that magnetic moments of two Co adatoms on clean Cu(111) at separations of 8 Å are aligned parallel to each other or, in other words, adatoms are coupled ferromagnetically. This statement is not necessarily true because this ferromagnetic order can be destroyed by thermal fluctuations. Phase transition from the magnetically ordered state with *infinite lifetime* to the magnetically disordered paramagnetic state occurs at the so-called critical temperature T_c. The loss (or blocking) of magnetization at a temperature $T_B > T_c$ is a gradual process characterized by a

relaxation time τ. Dependence of the blocking temperature T_B on time implies a strict condition on the method of investigation: the *real time* has to be taken into account. As a result, classical Monte Carlo (MC) approach is typically used in theoretical studies to obtain T_c. KMC method, which describes the evolution of the system in real time, must be applied for calculations of T_B. There is another advantage of the kMC method: it allows to perform theoretical simulations of realistic hysteresis loops at the given sweeping rate dB/dt of an externally applied magnetic field [110]. We describe the physical model of spin dynamics which is then solved by means of classical MC for computation of critical temperatures of close-packed magnetic chains and by means of kMC for studies of blocking temperatures of sparse magnetic chains.

5.1 The model of spin dynamics Let us consider a single finite chain of magnetic adatoms. Each atom i of the chain is characterized by the normalized spin value $\mathbf{s}_i$, $|\mathbf{s}_i| = 1$ and magnetic moment μ_i. The effective spin of the atom can, thus, be expressed as $(1/2)\mu_i\mathbf{s}_i$. If J_{ij} is the interaction between atoms i and j ($J<0$ for ferromagnetic exchange) and K is the magnetic anisotropy energy (MAE), then the spin dynamics of the system in the external magnetic field $\mathbf{B}$ aligned parallel to the direction $\mathbf{z}$ is described by the classical Heisenberg Hamiltonian [110]:

$$\mathcal{H} = \sum_{\langle i,j\rangle} J_{ij}\mathbf{s}_i \cdot \mathbf{s}_j - K\sum_i (\mathbf{s}_i \cdot \mathbf{z})^2 - \mu\mathbf{B} \cdot \sum_i \mathbf{s}_i, \qquad (10)$$

where $\langle i,j\rangle$ means summation over all neighbor spin pairs i and j and values of J_{ij} are taken for *normalized* spins. This model has recently been introduced and tested against experimental data by Vindigni et al. [111]. Spin dynamics of the system can be represented as a sequence of flips of magnetic moments $\mathbf{s}_i$ from the initial metastable state with energy $E_0^{(i)}$ to the final metastable state with energy $E_1^{(i)}$. In the conventional classical MC method a system can be switched from the initial to the final state with the probability determined by energies $E_0^{(i)}$ and $E_1^{(i)}$. Every flip event is only a part of the MC solution algorithm and drives the system into the equilibrium, but it cannot be treated as a time increment and has no physical meaning. The kMC method, on the contrary, allows to calculate the average time increment at each step [106].

5.2 Magnetic behavior in close-packed wires At first we consider magnetic interactions inside close-packed chains and wires [112]. To use a clear notation, chains are monatomic close-packed atomic structures, while wires are systems consisting of two parallel nearest neighbor chains. Mo et al. [8], and Guo et al. [9], revealed that Fe adatoms evaporated on the Cu(111) stepped surface self-organize themselves in chains embedded into the terrace as it is shown in Fig. 9. Such chains can serve as a template for growing, atop them, transition metal (TM) chains yielding mixed Fe-TM wires sketched in Fig. 9.

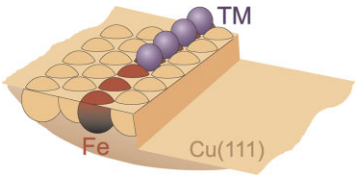

Figure 9 (online color at: www.pss-b.com) Sketch of the studied system. Red balls correspond to the infinite Fe chain embedded into the step edge of the Cu(111) surface. This chain serves as a nucleation template for growing the second transition metal (TM) chain sketched by blue balls on the upper terrace [112].

Ab initio investigations of the freestanding TM chains performed using Vienna Ab initio Simulation Package (VASP) [113–116] reveal that the nearest neighbor exchange interactions are the most important. Already the next-nearest neighbor interactions are an order of magnitude smaller. Therefore, we restrict the Heisenberg model to nearest neighbor interactions only. Exchange constants J_{ij} can be extracted from DFT calculations by comparison of total energies of several artificial noncollinear magnetic structures. The matter of this approach is to switch on or off particular interactions between atoms i and j by deliberate choice of noncollinear states when $\mathbf{s}_i \cdot \mathbf{s}_j = 0$. Noncollinear configurations used for calculation of the exchange parameters for freestanding and embedded wires are sketched in Fig. 10. The obtained exchange parameters for all the systems are given in Table 1. Some general

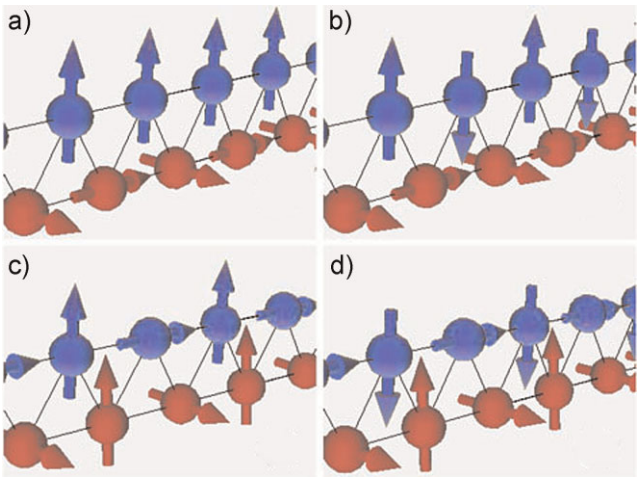

Figure 10 (online color at: www.pss-b.com) Noncollinear arrangement of spin moments used in calculations of exchange constants: (a and b) the spin moments at the Fe atoms (red) are oriented in a such direction that nearest-neighbor interactions between the Fe chain (red spins, bottom rows) and between Fe and the TM chain (blue spins, up rows) cancel each other in the Heisenberg Hamiltonian; J_{TM-TM} can be calculated. (c and d) Configurations which allow to calculate the interaction J_{TM-Fe} between the TM and Fe chains [112].

Table 1 Exchange constants for freestanding TM chains, freestanding TM-Fe wires, and embedded TM-Fe wires.

J (meV)	V	Cr	Mn	Fe	Co
freestanding chain					
J_{TM-TM}	−84	155	12	−106	−138
freestanding wire					
J_{TM-TM}	13	116	30	−80	−65
J_{TM-Fe}	80	26	−87	−150	−115
J_{Fe-Fe}	−48	−78	−82	−80	−54
embedded wire					
J_{TM-TM}	−22	70	26	−80	−67
J_{TM-Fe}	60	−18	−74	−80	−68
J_{Fe-Fe}	−65	−49	−58	−75	−56

The definition of the constants in the Heisenberg model incorporates the magnetic spin moments. $J<0$ corresponds to ferromagnetic coupling.

Table 2 Critical temperatures for the freestanding and embedded TM-Fe wires calculated by means of classical MC simulations for MAE K of 1.0 meV [117].

T_c (K)	V	Cr	Mn	Fe	Co
freestanding chain	100	20	132	68	75
embedded wire	88	41	63	122	94

conclusions can be drawn from these data. The exchange constants reflect the result that Fe–Fe and Co–Fe wires have ferromagnetic ground states. Antiferromagnetic couplings are present at the beginning of the 3D row. For the freestanding wires J_{Fe-Fe} is roughly constant throughout the series. Cr shows a strong antiferromagnetic intrachain coupling, whereas in V–Fe a strong antiferromagnetic interchain coupling is present. Relaxation effects are reflected in the exchange constants of the embedded systems. The stronger hybridization due to the inward relaxation of the TM chains leads to a decrease of the interchain exchange constants.

It is well known, that quantum fluctuations should drive T_c in pure 1D systems to 0. Our model, however, is effectively not 1D due to presence of the magnetic anisotropy and in such systems, as it has been demonstrated by Gambardella et al. [4], T_c is nonzero. Our classical MC simulations by means of Metropolis algorithm assuming for an atom $K=1$ meV indicate that critical temperatures of the systems are well below the room temperature [117] (Table 2). The critical temperature reaches its maximum for the Fe–Fe wire ($T_c=122$ K) [117].

5.3 Magnetic behavior of 1D sparse chains Now we would like to apply the kMC method developed in Ref. [110, 118] for spin dynamics, to examine blocking temperature of the 1D sparse nanostructures. Typically, such structures consist of individual atoms separated by 1–3 nm (see Figs. 6 and 8). The critical temperature in such weakly coupled systems is close to 0 K, but one can study the magnetization dynamics in *real time* by means of kMC to figure out the blocking temperature of the system. Surface state electrons governing self-organization of sparse chains also mediate the exchange interaction between the adatoms. Reasonable values of the exchange interaction J in our system can be estimated from the KKR *ab initio* studies and read $|J| \in [0\ldots1]$ meV, which is two orders smaller than in compact chains and wires (Section 5.2). In order to get the results relevant to the choice of K, the MAE was considered in the interval [0.1...1.2] meV. This is a reasonable interval of values of K [119]. Magnetic moment $\mu=3.2\,\mu_B$ corresponds to the magnetic moment of a Fe adatom on Cu(111) and is taken from our *ab initio* calculations.

Typical magnetization response of a 1D sparse atomic chain consisting of $N=100$ atoms to the external oscillating magnetic field is demonstrated in Fig. 11 [120]. The character of magnetization significantly depends on temperature. At $T=1$ K adatoms coupled with $J=-0.3$ meV exhibit a pronounced hysteresis with a coercive magnetic field (field at zero magnetization) $B_c=0.26$ T (Fig. 11a). If $J=0$ eV (Fig. 11a) or the temperature is increased to 2 K (Fig. 11b), the hysteresis disappears. It indicates that the blocking temperature of sparse 1D structures stabilized by the substrate-mediated interaction is about 1 K.

Figure 11c summarizes the study on the dependence of B_c on J and K at a temperature $T=0.5$ K [120]. From this figure one can see the onset of ferromagnetism in the whole range of values J and K considered in our study. Increasing J at a fixed K leads to an increase of B_c. Similarly, at a fixed J, larger values of B_c are reached at larger K.

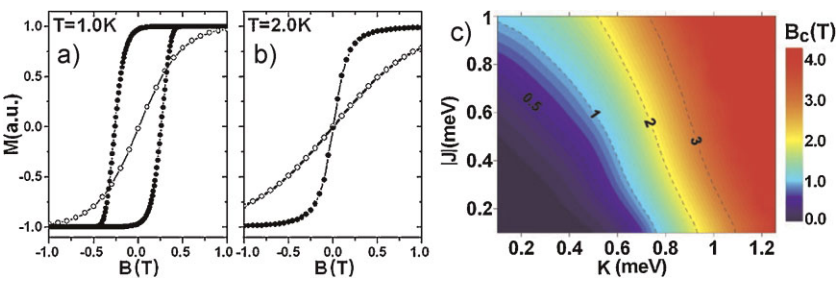

Figure 11 (online color at: www.pss-b.com) Magnetization response of the 1D sparse chain of $N=100$ atoms at (a) $T=1.0$ K, (b) $T=2.0$ K to the externally applied oscillating magnetic field. $K=1.0$ meV, $dB/dt\sim130$ T/s [110]. Filled black circles correspond to $J=-0.3$ meV, open gray to $J=0.0$ meV. (c) Coercive field B_c as a function of the MAE K and exchange coupling constant J. The data are calculated for the chain length $N=100$, $T=0.5$ K, and $dB/dt\sim130$ T/s [120].

6 Conclusions Presented results demonstrate various aspects of quantum phenomena in 1D metal atomic structures on metal substrates. It has been shown that despite the coupling to the substrate confined quantum-well-like states can still arise in the local projected band gaps of the substrate. The interaction of 1D chains with substrate-related surface states results in a formation of complex bound states. Surface states confined to 1D nanostructures, like chains, steps, or resonators, can be utilized for creation of sparse 1D nanostructures. This statement has been illustrated with several examples. Finally, we focused on the magnetization dynamics in sparse and compact 1D atomic structures and our studies revealed critical and blocking temperatures in the examined classes of systems.

Acknowledgements The financial support of Deutsche Forschungsgemeinschaft (SPP1165) is gratefully acknowledged. We thank Guntram Fischer (Martin-Luther-Universität Halle-Wittenberg) for his help in calculation of critical temperatures of TM-Fe wires (Section 5.2).

References

[1] H. Röder, E. Hahn, H. Brune, J.-P. Bucher, and K. Kern, Nature (London) **366**, 141 (1993).
[2] F. J. Himspel, J. E. Ortega, G. J. Mankey, and R. F. Willis, Adv. Phys. **47**, 511 (1998).
[3] P. Gambardella, M. Blanc, L. Bürgi, K. Kuhnke, and K. Kern, Surf. Sci. **449**, 93 (2000).
[4] P. Gambardella, M. Blanc, H. Brune, K. Kuhnke, and K. Kern, Phys. Rev. B **61**, 2254 (2000).
[5] P. Gambardella, A. Dallmeyer, K. Maiti, M. C. Malagoli, W. Eberhardt, K. Kern, and C. Carbone, Nature (London) **416**, 301 (2002).
[6] S. Shiraki, H. Fujisawa, T. Nakamura, T. Muro, M. Nantoh, and M. Kawai, Phys. Rev. Lett. **92**, 096102 (2004).
[7] O. V. Stepanyuk, N. N. Negulyaev, P. A. Ignatiev, M. Przybylski, W. Hergert, A. M. Saletsky, and J. Kirschner, Phys. Rev. B **79**, 155410 (2009).
[8] Y. Mo, K. Varga, E. Kaxiras, and Z. Zhang, Phys. Rev. Lett. **94**, 155503 (2005).
[9] J. Guo, Y. Mo, E. Kaxiras, Z. Zhang, and H. H. Weitering, Phys. Rev. B **73**, 193405 (2006).
[10] Y. Pennec, W. Auwärter, A. Schiffrin, A. Weber-Bargioni, A. Riemann, and J. V. Barth, Nat. Nanotechnol. **2**, 99 (2007).
[11] C. Liu, T. Uchihashi, and T. Nakayama, Phys. Rev. Lett. **101**, 146104 (2008).
[12] H. J. Elmers, J. Hauschild, H. Höche, U. Gradmann, H. Bethge, D. Heuer, and U. Köhler, Phys. Rev. Lett. **73**, 898 (1994).
[13] J. Shen, R. Skomski, M. Klaua, H. Jenniches, S. S. Manoharan, and J. Kirschner, Phys. Rev. B **56**, 2340 (1997).
[14] J. Shen, M. Klaua, P. Ohresser, H. Jenniches, J. Barthel, Ch. V. Mohan, and J. Kirschner, Phys. Rev. B **56**, 11134 (1997).
[15] N. N. Negulyaev, V. S. Stepanyuk, W. Hergert, P. Bruno, and J. Kirschner, Phys. Rev. B **77**, 085430 (2008).
[16] S. Shiraki, H. Fujisawa, T. Nakamura, T. Muro, M. Nantoh, and M. Kawai, Phys. Rev. B **78**, 115428 (2008).
[17] X.-D. Ma, D. I. Bazhanov, O. Fruchart, F. Yildiz, T. Yokoyama, M. Przybylski, V. S. Stepanyuk, W. Hergert, and J. Kirschner, Phys. Rev. Lett. **102**, 205503 (2009).
[18] C. Tegenkamp, J. Phys.: Condens. Matter **21**, 013002 (2009).
[19] H. Brune, H. Röder, C. Boragno, and K. Kern, Phys. Rev. Lett. **73**, 1955 (1994).
[20] K. Bromann, H. Brune, H. Röder, and K. Kern, Phys. Rev. Lett. **75**, 677 (1995).
[21] H. Brune, M. Giovannini, K. Bromann, and K. Kern, Nature (London) **394**, 451 (1998).
[22] J. E. Prieto, J. de la Figuera, and R. Miranda, Phys. Rev. B **62**, 2126 (2000).
[23] M. V. Rastei, B. Heinrich, L. Limot, P. A. Ignatiev, V. S. Stepanyuk, P. Bruno, and J. P. Bucher, Phys. Rev. Lett. **99**, 246102 (2007).
[24] M. Bachmann, M. Gabl, C. Deisl, N. Memmel, and E. Bertel, Phys. Rev. B **78**, 235410 (2008).
[25] M. Gabl, M. Bachmann, N. Memmel, and E. Bertel, Phys. Rev. B **79**, 153409 (2009).
[26] J. P. Pierce, M. A. Torija, Z. Gai, J. Shi, T. C. Schulthess, G. A. Farnan, J. F. Wendelken, E. W. Plummer, and J. Shen, Phys. Rev. Lett. **92**, 237201 (2004).
[27] M. A. Torija, A. P. Li, X. C. Guan, E. W. Plummer, and J. Shen, Phys. Rev. Lett. **93**, 257203 (2005).
[28] L. Yin, D. Xiao, Zh. Gai, T. Z. Ward, N. Widjaja, G. M. Stocks, Zh. Cheng, E. W. Plummer, Z. Zhang, and J. Shen, Phys. Rev. Lett. **104**, 167202 (2010).
[29] S. Rohart, V. Repain, A. Tejeda, P. Ohresser, F. Scheurer, P. Bencok, J. Ferrer, and S. Rousset, Phys. Rev. B **73**, 165412 (2006).
[30] R. Skomski, J. Zhang, V. Sessi, J. Honolka, A. Enders, and K. Kern, J. Appl. Phys. **103**, 07D519 (2008).
[31] Y. Nahas, V. Repain, C. Chacon, Y. Girard, J. Lagoute, G. Rodary, J. Klein, S. Rousset, H. Bulou, and C. Goyhenex, Phys. Rev. Lett. **103**, 067202 (2009).
[32] A. Kleibert, K.-H. Meiwes-Broer, and J. Bansmann, Phys. Rev. B **79**, 125423 (2009).
[33] J. V. Barth, G. Costantini, and K. Kern, Nature (London) **437**, 671 (2005).
[34] Z. Zhang and M. G. Lagally, Science **276**, 377 (1997).
[35] F. Silly, M. Pivetta, M. Ternes, F. Patthey, J. P. Pelz, and W.-D. Schneider, New J. Phys. **6**, 16 (2004).
[36] F. Silly, M. Pivetta, M. Ternes, F. Patthey, J. P. Pelz, and W.-D. Schneider, Phys. Rev. Lett. **92**, 016101 (2004).
[37] M. Ternes, C. Weber, M. Pivetta, F. Patthey, J. P. Pelz, T. Giamarchi, F. Mila, and W.-D. Schneider, Phys. Rev. Lett. **93**, 146805 (2004).
[38] M. Ternes, M. Pivetta, F. Patthey, and W.-D. Schneider, Prog. Surf. Sci. **85**, 1 (2010).
[39] P. Gambardella and K. Kern, Surf. Sci. **475**, L229 (2001).
[40] P. Gambardella, M. Blanc, K. Kuhnke, K. Kern, F. Picaud, C. Ramseyer, C. Girardet, C. Barreteau, D. Spanjaard, and M. C. Desjonquéres, Phys. Rev. B **64**, 045404 (2001).
[41] D. M. Eigler and E. K. Schweizer, Nature **344**, 524 (1990).
[42] M. F. Crommie, C. P. Lutz, and D. M. Eigler, Science **262**, 218 (1993).
[43] H. C. Manoharan, C. P. Lutz, and D. M. Eigler, Nature **403**, 512 (2000).
[44] N. Nilius, T. M. Wallis, and W. Ho, Science **297**, 1853 (2002).

[45] K.-F. Braun and K.-H. Rieder, Phys. Rev. Lett. **88**, 096801 (2002).
[46] S.-W. Hla, K.-F. Braun, and K.-H. Rieder, Phys. Rev. B **67**, 201402R (2003).
[47] S. Fölsch, P. Hyldgaard, R. Koch, and K. H. Ploog, Phys. Rev. Lett. **92**, 056803 (2004).
[48] C. F. Hirjibehedin, C. P. Lutz, and A. J. Heinrich, Science **312**, 1021 (2006).
[49] J. Lagoute, C. Nacci, and S. Fölsch, Phys. Rev. Lett. **98**, 146804 (2007).
[50] M. F. Crommie, C. P. Lutz, and D. M. Eigler, Nature **363**, 524 (1993).
[51] Y. Hasegawa and P. Avouris, Phys. Rev. Lett. **71**, 1071 (1993).
[52] L. Petersen, P. Laitenberger, E. Lægsgaard, and F. Besenbacher, Phys. Rev. B **58**, 7361 (1998).
[53] J. T. Li, W.-D. Schneider, R. Berndt, and S. Crampin, Phys. Rev. Lett. **80**, 3332 (1998).
[54] J. V. Barth, H. Brune, G. Ertl, and R. J. Behm, Phys. Rev. B **42**, 9307 (1990).
[55] L. Diekhöner, M. A. Schneider, A. N. Baranov, V. S. Stepanyuk, P. Bruno, and K. Kern, Phys. Rev. Lett. **90**, 236801 (2003).
[56] O. Pietzsch, S. Okatov, A. Kubetzka, M. Bode, S. Heinze, A. Lichtenstein, and R. Wiesendanger, Phys. Rev. Lett. **96**, 237203 (2006).
[57] F. Meier, K. von Bergmann, P. Ferriani, J. Wiebe, M. Bode, K. Hashimoto, S. Heinze, and R. Wiesendanger, Phys. Rev. B **74**, 195411 (2006).
[58] H. Oka, P. A. Ignatiev, S. Wedekind, G. Rodary, L. Niebergall, V. S. Stepanyuk, D. Sander, and J. Kirschner, Science **327**, 843 (2010).
[59] F. Meier, L. Zhou, J. Wiebe, and R. Wiesendanger, Science **320**, 82 (2008).
[60] J. Zabloudil, R. Hammerling, L. Szunyogh, and P. Weinberger, Electron Scattering in Solid Matter: A Theoretical and Computational Treatise, Springer Series in Solid-State Sciences, Vol. 147 (Springer Verlag, Berlin, 2005).
[61] K. Wildberger, V. S. Stepanyuk, P. Lang, R. Zeller, and P. H. Dederichs, Phys. Rev. Lett. **75**, 509 (1995).
[62] V. S. Stepanyuk, W. Hergert, K. Wildberger, R. Zeller, and P. H. Dederichs, Phys. Rev. B **53**, 2121 (1996).
[63] R. Zeller, P. H. Dederichs, B. Újfalussy, L. Szunyogh, and P. Weinberger, Phys. Rev. B **52**, 8807 (1995).
[64] V. S. Stepanyuk, L. Niebergall, W. Hergert, and P. Bruno, Phys. Rev. Lett. **94**, 187201 (2005).
[65] V. S. Stepanyuk, L. Niebergall, R. C. Longo, W. Hergert, and P. Bruno, Phys. Rev. B **70**, 075414 (2004).
[66] J. Dorantes-Dávila and G. M. Pastor, Phys. Rev. Lett. **81**, 208 (1998).
[67] R. Félix-Medina, J. Dorantes-Dávila, and G. M. Pastor, Phys. Rev. B **67**, 094430 (2003).
[68] Š. Pick, P. A. Ignatiev, A. L. Klavsyuk, W. Hergert, V. S. Stepanyuk, and P. Bruno, J. Phys.: Condens. Matter **19**, 446001 (2007).
[69] A. B. Klautau and S. Frota-Pessoa, Phys. Rev. B **70**, 193407 (2004).
[70] M. Persson, Phys. Rev. B **70**, 205420 (2004).
[71] P. H. Zhou, P. Moras, L. Ferrari, G. Bihlmayer, S. Blügel, and C. Carbone, Phys. Rev. B **70**, 205420 (2004).
[72] S. Díaz-Tendero, F. E. Olsson, A. G. Borisov, and J.-P. Gauyacq, Phys. Rev. B **79**, 115438 (2009).
[73] S. Díaz-Tendero, A. G. Borisov, and J.-P. Gauyacq, Phys. Rev. Lett. **102**, 166807 (2009).
[74] N. Memmel, Surf. Sci. Rep. **32**, 91 (1998).
[75] S. G. Davison and M. Steslicka, Basic Theory of Surface States (Clarendon Press, Oxford; Oxford University Press, New York, 1992).
[76] F. Reinert, G. Nicolay, S. Schmidt, D. Ehm, and S. Hüfner, Phys. Rev. B **63**, 115415 (2001).
[77] D. M. Newns, Phys. Rev. **178**, 1123 (1969).
[78] L. Limot, E. Pehlke, J. Kröger, and R. Berndt, Phys. Rev. Lett. **94**, 036805 (2005).
[79] V. S. Stepanyuk, A. N. Klavsyuk, L. Niebergall, and P. Bruno, Phys. Rev. B **72**, 153407 (2005).
[80] J. P. Gauyacq, A. G. Borisov, and A. K. Kazansky, Appl. Phys. A **78**, 141 (2004).
[81] K. H. Lau and W. Kohn, Surf. Sci. **75**, 69 (1978).
[82] P. Hyldgaard and M. Persson, J. Phys.: Condens. Matter **12**, L13 (2000).
[83] O. O. Brovko, P. A. Ignatiev, V. S. Stepanyuk, and P. Bruno, Phys. Rev. Lett. **101**, 036809 (2008).
[84] W. Chen, T. Jamneala, V. Madhavan, and M. F. Crommie, Phys. Rev. B **60**, 8529R (1999).
[85] P. Wahl, P. Simon, L. Diekhöner, V. S. Stepanyuk, P. Bruno, M. A. Schneider, and K. Kern, Phys. Rev. Lett. **98**, 056601 (2007).
[86] P. A. Ignatiev, N. N. Negulyaev, A. S. Smirnov, L. Niebergall, A. M. Saletsky, and V. S. Stepanyuk, Phys. Rev. B **80**, 165408 (2009).
[87] V. S. Stepanyuk, A. N. Baranov, D. V. Tsivlin, W. Hergert, P. Bruno, N. Knorr, M. A. Schneider, and K. Kern, Phys. Rev. B **68**, 205410 (2003).
[88] J. Repp, F. Moresco, G. Meyer, K.-H. Rieder, P. Hyldgaard, and M. Persson, Phys. Rev. Lett. **85**, 2981 (2000).
[89] N. Knorr, H. Brune, M. Epple, A. Hirstein, M. A. Schneider, and K. Kern, Phys. Rev. B **65**, 115420 (2002).
[90] X. P. Zhang, B. F. Miao, L. Sun, C. L. Gao, An Hu, H. F. Ding, and J. Kirschner, Phys. Rev. B **81**, 125438 (2010).
[91] M. Ziegler, J. Kröger, R. Berndt, A. Filinov, and M. Bonitz, Phys. Rev. B **78**, 245427 (2008).
[92] S. U. Nanayakkara, E. C. H. Sykes, L. C. Fernández-Torres, M. M. Blake, and P. S. Weiss, Phys. Rev. Lett. **98**, 206108 (2007).
[93] N. N. Negulyaev, V. S. Stepanyuk, L. Niebergall, P. Bruno, W. Auwärter, Y. Pennec, G. Jahnz, and J. V. Barth, Phys. Rev. B **79**, 195411 (2009).
[94] G. Manai, K. Radican, F. Delogu, and I. V. Shvets, Phys. Rev. Lett. **101**, 165701 (2008).
[95] V. S. Stepanyuk, N. N. Negulyaev, L. Niebergall, R. C. Longo, and P. Bruno, Phys. Rev. Lett. **97**, 186403 (2006).
[96] V. S. Stepanyuk, N. N. Negulyaev, L. Niebergall, and P. Bruno, New J. Phys. **9**, 388 (2007).
[97] N. N. Negulyaev, V. S. Stepanyuk, L. Niebergall, P. Bruno, M. Pivetta, M. Ternes, F. Patthey, and W.-D. Schneider, Phys. Rev. Lett. **102**, 246102 (2009).
[98] H. F. Ding, V. S. Stepanyuk, P. A. Ignatiev, N. N. Negulyaev, L. Niebergall, M. Wasniowska, C. L. Gao, P. Bruno, and J. Kirschner, Phys. Rev. B **76**, 033409 (2007).
[99] K. A. Fichthorn and M. Scheffler, Phys. Rev. Lett. **84**, 5371 (2000).
[100] K. A. Fichthorn, M. L. Merrick, and M. Scheffler, Appl. Phys. A **75**, 17 (2002).

[101] K. A. Fichthorn, M. L. Merrick, and M. Scheffler, Phys. Rev. B **68**, 041404R (2003).
[102] J. M. Rogowska and M. Maciejewski, Phys. Rev. B **74**, 235402 (2006).
[103] J. Hu, B. Teng, F. Wu, and Y. Fang, New J. Phys. **10**, 023033 (2008).
[104] N. N. Negulyaev, V. S. Stepanyuk, L. Niebergall, P. Bruno, W. Hergert, J. Repp, K.-H. Rieder, and G. Meyer, Phys. Rev. Lett. **101**, 226601 (2008).
[105] R. Smoluchowski, Phys. Rev. **60**, 661 (1941).
[106] K. A. Fichthorn and W. H. Weinberg, J. Chem. Phys. **95**, 1090 (1991).
[107] L. Bürgi, O. Jeandupeux, A. Hirstein, H. Brune, and K. Kern, Phys. Rev. Lett. **81**, 5370 (1998).
[108] A. Schiffrin, J. Reichert, W. Auwärter, G. Jahnz, Y. Pennec, A. Weber-Bargioni, V. S. Stepanyuk, L. Niebergall, P. Bruno, and J. V. Barth, Phys. Rev. B **78**, 035424 (2008).
[109] A. Schiffrin, A. Riemann, W. Auwärter, Y. Pennec, A. Weber-Bargioni, D. Cvetko, A. Cossaro, M. Alberto, and J. V. Barth, Proc. Natl. Acad. Sci. USA **104**, 5279 (2007).
[110] Y. Li and B.-G. Liu, Phys. Rev. B **73**, 174418 (2006).
[111] A. Vindigni, A. Rettori, M. G. Pini, C. Carbone, and P. Gambardella, Appl. Phys. A **82**, 385 (2006).
[112] H. Hashemi, W. Hergert, and V. S. Stepanyuk, Phys. Rev. B **81**, 104418 (2010).
[113] G. Kresse and J. Hafner, Phys. Rev. B **47**, 558 (1993).
[114] G. Kresse and J. Furthmüller, Phys. Rev. B **54**, 11169 (1996).
[115] G. Kresse and J. Furthmüller, Comput. Mater. Sci. **6**, 15 (1996).
[116] G. Kresse and D. Joubert, Phys. Rev. B **59**, 1758 (1999).
[117] H. Hashemi, G. Fischer, W. Hergert, and V. S. Stepanyuk, J. Appl. Phys. **107**, 09E311 (02010).
[118] R. J. Glauber, J. Math. Phys. **4**, 294 (1963).
[119] Š. Pick, V. S. Stepanyuk, A. L. Klavsyuk, L. Niebergall, W. Hergert, J. Kirschner, and P. Bruno, Phys. Rev. B **70**, 224419 (2004).
[120] A. S. Smirnov, N. N. Negulyaev, W. Hergert, A. M. Saletsky, and V. S. Stepanyuk, New J. Phys. **11**, 063004 (2009).